Clays and Clay Minerals, Vol. 61, No. 3, 177–192, 2013.

ZEOLITES IN MAFIC PYROCLASTIC ROCKS FROM THE SANDIKLI-AFYONKARAHISAR REGION, TURKEY

YAHYA OZPINAR[1], BARIS SEMIZ[1,*], AND PAUL A. SCHROEDER[2]

[1] Pamukkale University, Department of Geological Engineering, TR-20070, Denizli, Turkey
[2] The University of Georgia, Department of Geology, Athens, GA 30602-2501, USA

Abstract—Geologic mapping and crystal-chemical analysis of Middle–Upper Miocene volcanics in the Sandıklı-Afyonkarahisar region of Turkey, coupled with published zeolite analyses has revealed that western Turkey hosts unique zeolitic mineral assemblages with distinct paragenetic sequences. The present investigation focused on pyroclastic deposits, including low to intermediate potassic trachytic/trachyandesitic tuffs (LPT) and high potassic tephriphonolitic, tephritic, and trachybasaltic tuffs (HPT), each of which contains various styles of zeolites. Optical petrography, X-ray powder diffraction, and chemical analyses have revealed varying degrees of lithification, probably related to differences in initial emplacement temperature, depositional mechanism and thickness, chilling rate, and extent of mafic composition. Zeolitization was further influenced by meteoric flushing in a hydrologically open system. Chabazite in the LPT from the Selçik area occurs extensively as coatings and infillings of pores. Phillipsite in the HPT found in the Ballık, Küfeke, and Ömerkuyu areas dominates the assemblage and is accompanied by chabazite and minor amounts of analcime. Analcime was probably generated by alteration of leucite which is found as a pyrogene mineral. Alkali zeolites or Ca-bearing zeolites formed as a consequence of the addition of Ca and/or the removal of Na (*i.e.* dissolution of analcime). The paragenetic sequence may be described as: analcime/phillipsite → chabazite → calcite. The characterization of these assemblages may lead to better exploitation strategies for natural zeolitic resources in the region.

Key Words—Alkaline Pyroclastic Rocks, Chabazite, Phillipsite, Sandıklı, Western Anatolia, Zeolites.

INTRODUCTION

Zeolite occurrences in western Anatolia, Turkey, are normally related to felsic/acidic volcanism formed in saline-alkaline lake basins, which often contain borates, K-feldspar, carbonates, and clay minerals. In Turkey, these occurrences include the regions of Bigadiç, Kırka, Gördes, Simav, Emet, Alaçatı (Çeşme), and Ayvacık-Küçükkuyu (Çanakkale) (Helvacı *et al.*, 1993; Gündoğdu *et al.*, 1996; Kaçmaz and Koktürk, 2004; Esenli and Sirkecioğlu, 2005; Snellings *et al.*, 2008; Semiz *et al.*, 2011; Özen and Göncüoğlu, 2011). Some of these zeolites, such as those in Gördes, are commercially exploited. Commonly, these zeolites are related to felsic and high-silica volcanism and include clinoptilolite, heulandite, analcime, mordenite, erionite, and phillipsite in the mineral assemblages (Bish and Carey, 2001). Zeolite-bearing pyroclastic rocks related to mafic or basaltic volcanism in Turkey are less common and have only recently been recognized (by Özpınar *et al.*, 2002) in the Sandıklı region, and in the Eastern Pontides (by Abdioğlu, 2012). Sandıklı zeolite occurrences are associated with trachytic, trachyandesitic, phonolitic, and tephriphonolitic pyroclastic deposits (Özpınar *et al.*, 2002; Özpınar, 2008, 2011). Similar occurrences are described in other locations around the world such as in Campi Flegrei in southern Italy (de' Gennaro *et al.*, 1999, 2000; Cappelletti *et al.*, 2003); the Canary Islands, Spain (Hernandez *et al.*, 1993); and in the Eifel region of Germany (Bernhard and Barth-Wirsching, 2002). Most of these deposits have been involved in alteration processes that led to the crystallization of phillipsite, chabazite, and analcime (de' Gennaro *et al.*, 1999, 2000). The purpose of the present study was to describe the occurrences of analcime-, chabazite-, and phillipsite-bearing rocks in the southeastern region of Sandıklı–Afyonkarahisar (western Anatolia, Turkey) hosted in mafic volcanics and to compare and contrast the deposits with others in the region and around the world. The broader implication of this work is the constraints these minerals can provide for better understanding of western Turkey geology and the exploitation potential of natural zeolitic resources.

MATERIALS AND METHODS

Detailed geologic field mapping of Sandıklı volcanics was conducted at a scale of 1/25,000 over an area of ~60 km^2 (Figure 1). Thin sections were prepared from 198 representative rock samples. The mineralogy of 58 bulk samples was determined by powder X-ray diffraction (XRD) using a Rigaku D/Max 2200 Ultima/PC diffractometer (in Turkey) and a Bruker D8 Advance diffractometer (in the USA). All powder samples were prepared using an automatic agate mortar. Most of the

* E-mail address of corresponding author:
bsemiz@pau.edu.tr
DOI: 10.1346/CCMN.2013.0610302

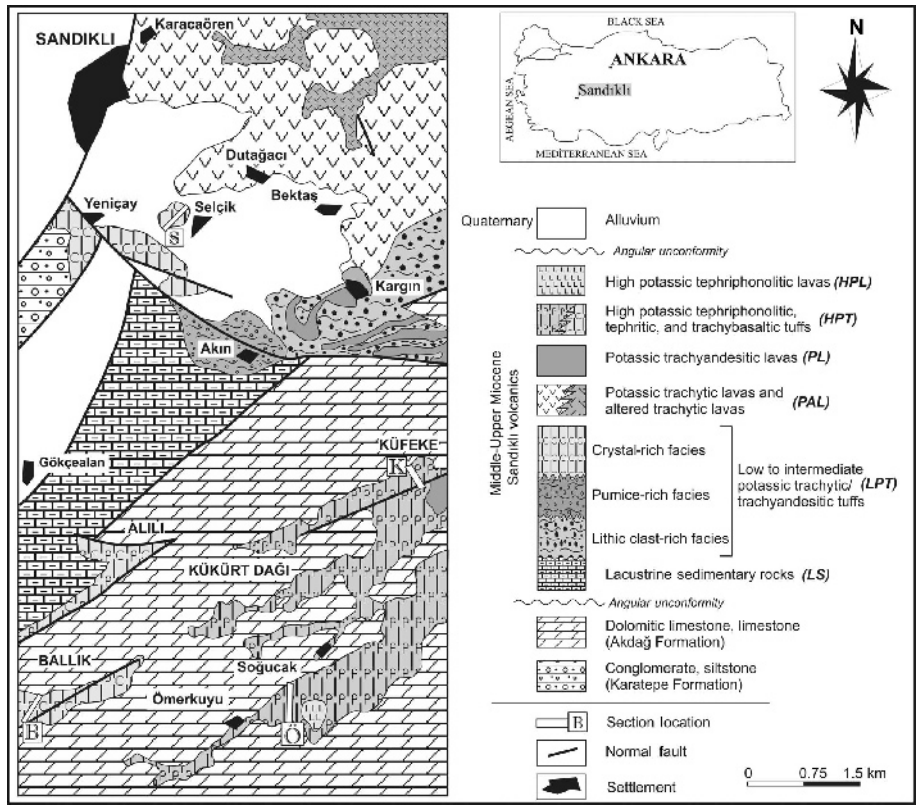

Figure 1. Geologic map of the Sandıklı volcanics.

pressed powders were scanned from 2 to 50º2θ at a rate of 1º/min using CuKα radiation (Ni-filtered). The other samples were measured at a continuous scan rate of 1.00º min^{-1} over a range of 2−70º2θ; counts were collected for 0.600 s at step increments of 0.010º with CoKα radiation (Ni filter).

Scanning electron microscopy and energy-dispersive spectroscopy (SEM-EDX) were used to characterize crystal morphologies. The SEM-EDX work was carried out at the Center for Advanced Ultrastructural Research (CAUR) at the University of Georgia, Athens, Georgia, USA, using a Zeiss 1450EP. Samples for SEM-EDX analysis were prepared by adhering a freshly broken surface of the sample onto an aluminum stub with double-sided tape, which was then coated with a carbon film (~350 Å) using an SPI Module Sputter Coater. Representative minerals of zeolitic tuffs were analyzed chemically by wavelength dispersive spectroscopy (WDS) using a JEOL 8600 electron microprobe at the University of Georgia, USA. Natural and synthetic mineral standards were analyzed as primary standards to monitor accuracy and precision. The WDS running conditions used a 15 kV accelerating voltage, a 15 nA beam current, and an analytical spot size of ~1 μm. The X-ray intensities were corrected using the Phi-Rho-Z matrix correction software of Armstrong (1988).

Bulk chemical analysis of 12 samples for major, trace, and rare earth elements (*REE*) analyses were carried out with fusion inductively coupled plasma (ICP) and fusion inductively coupled plasma-mass spectrometry (ICP-MS) in ACME Laboratories Ltd., Canada. The loss-on-ignition (LOI), representing the weight percentage of total water and volatile components, was determined by heating the samples to 1000ºC after drying them at 105±5ºC.

GEOLOGICAL FRAMEWORK

Basement rocks of the Neogene volcano-sedimentary units in the study area include the Upper Triassic–Lower Jurassic Karatepe Formation and Upper Jurassic−Lower Cretaceous Akdağ Formation. Basement rocks occur unconformably overlain by the Middle−Upper Miocene volcano-sedimentary sequence known as the Sandıklı Volcanics (Figure 1). The Sandıklı volcanic sequence is described as: (1) lacustrine sedimentary rocks (hereafter LS), which include conglomerates, sandstones, marls, and limestones; (2) low-to-intermediate potassic trachytic/ trachyandesitic tuffs (hereafter LPT); (3) trachytic lavas and partly altered trachytic lavas (hereafter PAL); (4) potassic trachyandesitic lavas (hereafter PL); (5) high potassic tephriphonolitic, tephritic, and

https://doi.org/10.1346/CCMN.2013.0610302 Published online by Cambridge University Press

trachybasaltic tuffs (hereafter HPT); and (6) high potassic tephriphonolitic lavas (hereafter HPL). They have been dated using the K-Ar method and give model ages of 8.0±0.6 and 14±0.3 Ma (Besang *et al.*, 1977; Ercan, 1986). These Miocene and older units are sporadically overlain by Quaternary alluvium (Figure 1).

Tuffs are divided into two groups on the basis of mineralogical properties and stratigraphic position. The lower group of tuffs (LPT) crops out around the villages of Selçik, Akin, and Yeniçay (Figure 1). The LPT in the Selçik-Akin area are beige in color and can be further divided into three sub-facies which include: (1) lithic clast-rich facies; (2) a pumice-rich facies; and (3) crystal-rich facies (Figure 2a). The lithic clast-rich facies is characterized by poorly sorted beds. These facies contain coarse-grained pyroclastics such as lapilli breccia and lapillistone, which appear as trachytic/trachyandesitic rock and white-gray pumice pieces. According to the classification of Schmid (1981), the upper part of this facies contains tuffaceous conglomerates, tuffaceous sandstones, tuffaceous siltstones, and tuffaceous mudstones. The pumice-rich facies consist of abundant, well rounded pumice clasts with different dimensions set in a poorly sorted ash matrix. This facies has a texture similar to that of ignimbrites and contains coarse-grained trachytic and trachyandesitic pyroclasts. The contacts between the upper and lower facies are gradational. The crystal-rich facies consist chiefly of varicolored, zeolitized, mostly fine-grained, vitric-crystal, and crystal vitric-tuffs. They are beige in color and contain variable amounts of small volcanic rock fragments and a few small epiclasts. Tuffs with zeolite are less lithified and contain chabazite. The zeolite content is greater in the uppermost levels. The depositional characteristics of LPT indicate strongly that they are ash-fall deposits.

The upper group crops out around the villages of Alılı, Ballık, Ömerkuyu, Soğucak, and Küfeke in the southern part of the study area (Figure 1). The HPT in the Ömerkuyu-Soğucak area unconformably overlie the Upper Jurassic to Lower Cretaceous Akdağ Formation (Figure 2b). The HPT have a brown, reddish brown, sometimes light brown color and are very well lithified. They are more dense than the chabazite-bearing trachytic tuffs and often contain volcanic rock fragments (pyroclasts) with fine to coarse sand, as well as a few small, partly rounded radiolarite and limestone fragments. The tuffs in Soğucak contain gravel and coarse sand-sized particles of basaltic and tephriphonolitic composition. Iron alteration appears to be greatest in this suite. Tuffs in Küfeke have fewer pyrogenic minerals and contain microcrystalline limestone "micrite" (Folk, 1962) and pumice (Figure 2c). The HPT contain chabazite and phillipsite near Alılı and Ballık, while phillipsite only occurs near Ömerkuyu, Soğucak, and Küfeke. The HPT appear to be ash-flow deposits.

RESULTS

Petrography-mineralogy

The mineralogical composition of the tuffs was determined by XRD analysis (Table 1). Zeolite minerals occur to a lesser extent in the low to intermediate potassic trachytic and trachyandesitic tuffs (LPT) and more extensively in the high potassic tephriphonolitic, tephritic, and trachybasaltic tuffs (HPT). The LPT contain chabazite, sanidine, and quartz, with minor

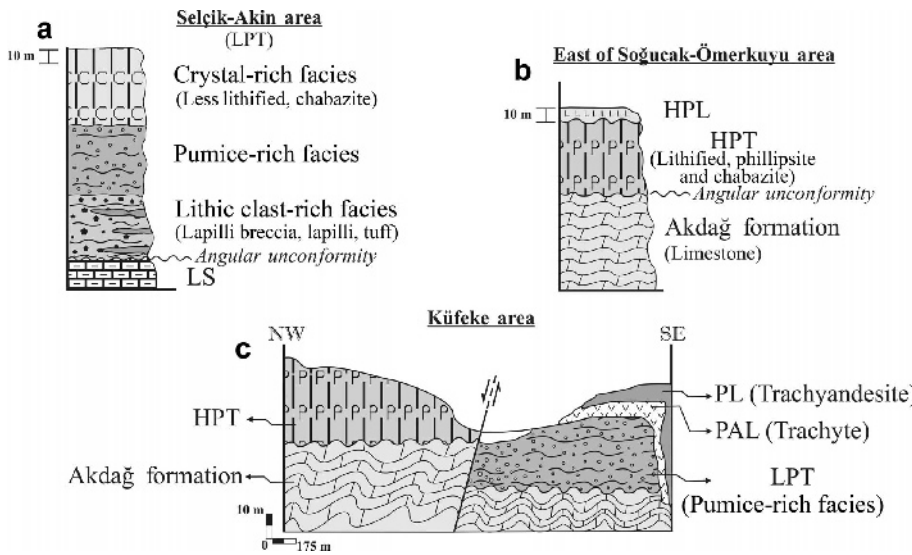

Figure 2. Stratigraphic position of pyroclastic rocks located in the study area: (a) trachytic tuffs (LPT) located in the Selçik and Akin areas; (b) tephriphonolitic tuffs (HPT) located east of the Soğucak-Ömerkuyu areas; and (c) relationship between the trachytic and tephriphonolitic tuffs (LPT and HPT) located in the Küfeke area.

https://doi.org/10.1346/CCMN.2013.0610302 Published online by Cambridge University Press

Table 1. Mineralogical composition of the LPT and HPT samples determined by powder XRD.

Rock type	Sample no	Locations	Minerals							
			Cha	Phi	Ana	San	Q	Cal	Bio	Aug
LPT	S11–S19	West of Selçik	+	–	–	+	+	–	–	–
LPT	S3–S4	West of Selçik	+	–	–	+	–	–	–	–
LPT	S34; S36	South of Selçik	+	–	–	+	+	+	–	–
LPT	S35	South of Selçik	+	–	–	+	+	–	–	–
LPT	S35; S37–S38	South of Selçik	+	–	–	+	+	–	–	–
LPT	S5– S5/1	South of Selçik	–	–	–	+	+	+	–	–
HPT	B20; B21	South of Ballık	–	+	–	–	–	+	–	–
HPT	B22–B24	South of Ballık	–	+	–	+	–	–	–	+
HPT	B6	Alılı	–	+	+	–	–	–	–	–
HPT	B31	South of Ballık	+	–	–	+	–	–	–	–
HPT	B303	South of Ballık	+	+	–	+	–	–	+	–
HPT	K32; K33	Küfeke	+	–	–	+	+	–	–	–
HPT	K22	Küfeke	–	+	+	–	–	–	–	–
HPT	K23	Küfeke	+	–	–	+	–	–	–	–
HPT	K335	Küfeke	+	+	–	–	–	+	+	–
HPT	O25	West of Ömer-kuyu	–	+	–	–	–	+	–	–
HPT	O26; O27	South of Soğucak	–	+	–	+	–	–	–	+
HPT	K28	Küfeke	–	+	–	–	–	+	–	–
HPT	K29; K31	Küfeke	–	+	–	+	–	–	–	+
HPT	K30	Küfeke	–	+	–	+	–	+	–	+
HPT	O313	Soğucak	–	+	–	+	–	–	+	–
Purified zeolites samples										
LPT	SZ2; SZ6	Selçik	+	–	–	+	+	+	–	–
LPT	SZ3	Selçik	+	–	–	+	+	–	–	–
LPT	SZ8	Selçik	+	–	–	+	–	–	–	–
HPT	OZ5	Soğucak	–	+	–	+	–	–	–	–
HPT	OZ7	Soğucak	–	+	–	–	–	+	–	–
HPT	OZ22/2	Soğucak	–	–	–	+	–	+	–	–
HPT	BZ1; BZ4	Ballık	+	+	–	–	–	+	–	–

Cha; chabazite, Phi; phillipsite, Ana; analcime, San; sanidine, Q; Quartz, Cal; calcite, Bio; Biotite, Aug; augite.

amounts of calcite (Figure 3a; Table 1). The LPT has variable, small pyroclasts with microlitic and micro-porphyritic textures. Although biotite, chlorite, and opaque minerals were not detected by XRD, they are occasionally observed by optical microscopy. Plagioclase and augite were also found as microlite and phenocrysts in the pyroclasts. The LPT is less lithified, containing many cavities and pores, resulting in greater porosities than the HPT. The HPT contain phillipsite, chabazite, sanidine, and minor amounts of analcime, calcite, biotite, and augite (Figure 3b,c; Table 1). Although chlorite and opaque minerals were not detected by XRD, they are occasionally determined by optical microscopy. The XRD patterns contain a broad background, which is interpreted to be a glassy matrix. Small amounts of analcime were found in two samples (B6 and B22) from the Alılı and Küfeke areas. A representative XRD pattern of a sample with analcime (B6) is shown in Figure 3d.

Chabazite is confined to the vesicles and appears as transparent crystal aggregates. Chabazite rhombohedra grew on phillipsite rims. Generally, chabazite is found together with calcite and grown in pyroclasts including remnant leucite forms (Figure 4a). The rhombohedra range from 10 to 30 μm in diameter. Phillipsite is always found as a thin rim inside the vesicles. Phillipsite occurs mainly as white rosettes of radiating and spherulitic crystal aggregates (Figure 4c). Phillipsite is also present as isolated stout euhedral prisms. Crystals range from 30 to 60 μm in length and spherulites are 50 μm in diameter. The smallest phillipsite crystals were found to have formed with alteration of volcanic glass and in the vitric-rich fragments located in HPT (Figures 4b). Phillipsite is occasionally found within cracks of sanidine and leucite, and around the leucite crystals (Figure 4c–d). Calcite occurs as coarse-grained cements filling central parts of vesicles and intergranular spaces. Calcite appears to have formed as the latest secondary mineral (Figure 4a).

Large leucite crystals (1–2 cm) were hand picked for XRD investigation from HPT and HPL. The XRD data indicated that analcime formed in the HPT and generally

https://doi.org/10.1346/CCMN.2013.0610302 Published online by Cambridge University Press

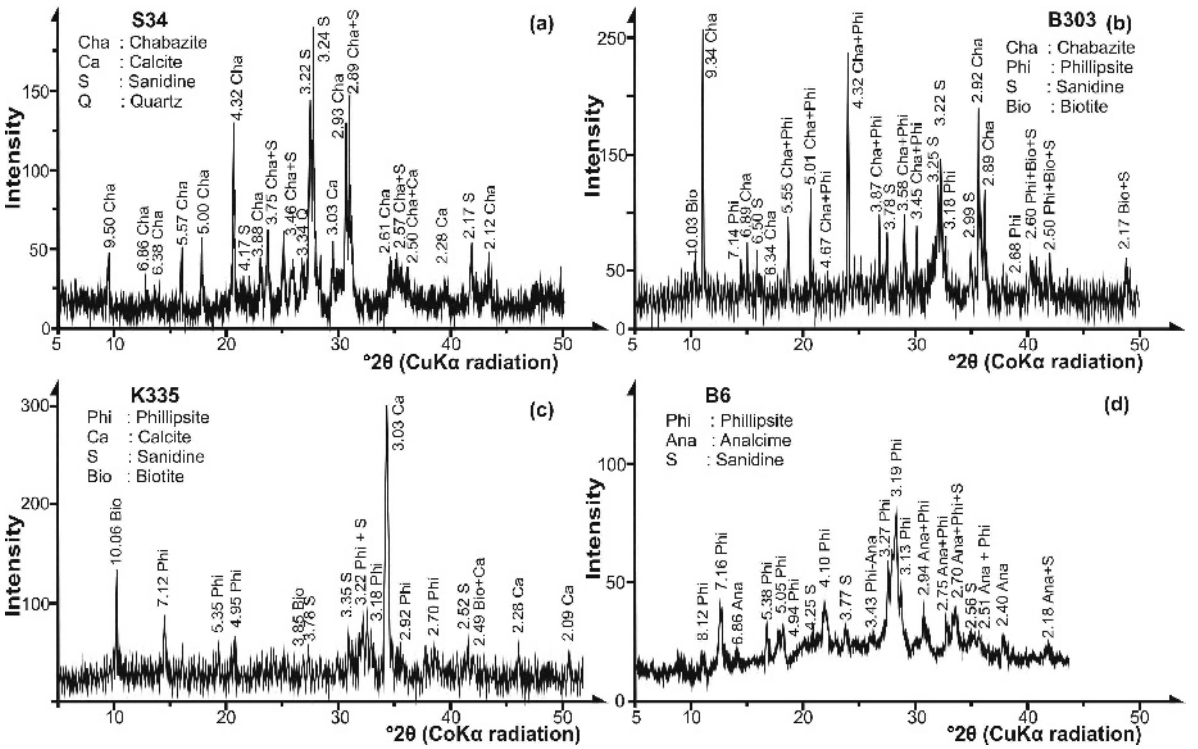

Figure 3. Mineralogical composition of the samples determined by XRD using CuKα and CoKα radiation. (a) LPT in the Selçik area (sample no. S34), (b) HPT in the Ballık area (sample no. B303), (c) HPT in the Küfeke area (sample no. K335), (d) HPT in the Alılı area (sample no. B6).

occurs together with leucite, which is found as a pyrogene mineral (Figure 5a) and leucite replacement by analcime. Analcime was probably formed by alteration of volcanic glass and of leucite. Analcime did not crystallize directly from a silicate melt and was not detected in the leucite crystal taken from HPL (Figure 5b). These rocks reveal an abundance of sanidine and leucite minerals.

The zeolite minerals were concentrated from zeolitic tuff by using heavy liquid (tetrabromoethane) (as per Minato, 1992). The small particulates (<2 μm) were dispersed in distilled water by ultrasonic vibration in a beaker and then filtered and dried at 60ºC. Zeolite particles were separated from the suspended small particulates using the heavy liquid tetrabromoethane. Concentrated zeolite grains were filtered on filter paper (Whatman™ Grade 541), washed with acetone, and dried. In the purified zeolite samples, XRD analysis showed the presence of chabazite and sanidine minerals in LPT (Figure 5c) and chabazite, phillipsite, and calcite minerals in HPT (Figure 5d). The zeolite content is defined as the weight percent retained during the separation process. The zeolite content in LPT (in the Selçik area) is up to 25 wt.% (Figure 6b). The zeolite content in HPT (in other areas) reaches up to 70 wt.% (Figure 6a,c,d). The zeolite content of the tuffs also varies vertically through the section. The LPT contains a maximum of 25% pyrogene minerals (sanidine, quartz, biotite, and ±augite) and the HPT contains a maximum of 8% pyrogene minerals (leucite, clinopyroxene, ±sanidine, and ±phlogopite).

Scanning electron microscopy and electron microprobe

Scanning electron microscopy (SEM) combined with energy-dispersive X-ray analysis (EDX) was carried out for all samples from HPT. Chabazite and phillipsite were the most abundant zeolite minerals observed (Figure 7a,b).

Chabazite appears as grouped rhombohedral crystals, often exhibiting 'pseudocubic' habit. Crystals from the study areas range in dimensions from 10 to 30 μm. Chabazite from the Ballık area, as in Figure 7a, formed in volcanic glass and cavities with dimensions ranging between 2 and 20 μm. The EDX analysis of chabazite crystals indicates a large Ca content in both sites (Figure 7a). Chabazite and phillipsite often occur together (Figure 7b). Phillipsite displays a spherulitic, radiating prismatic crystal habit infilling pores and ranges from 30 to 60 μm long, with a few of the crystals up to 120 μm long. Radiating prismatic K- and Ca-bearing phillipsite crystals from the Küfeke area are shown in Figure 7b. The EDX analysis revealed that all crystals contain mainly Si, Al, Ca, and K, similar to those observed by Tschernich (1992), but also contain minor amounts of Fe and Mg. Analcime occurrences are restricted to the Ballık and Küfeke localities. They

https://doi.org/10.1346/CCMN.2013.0610302 Published online by Cambridge University Press

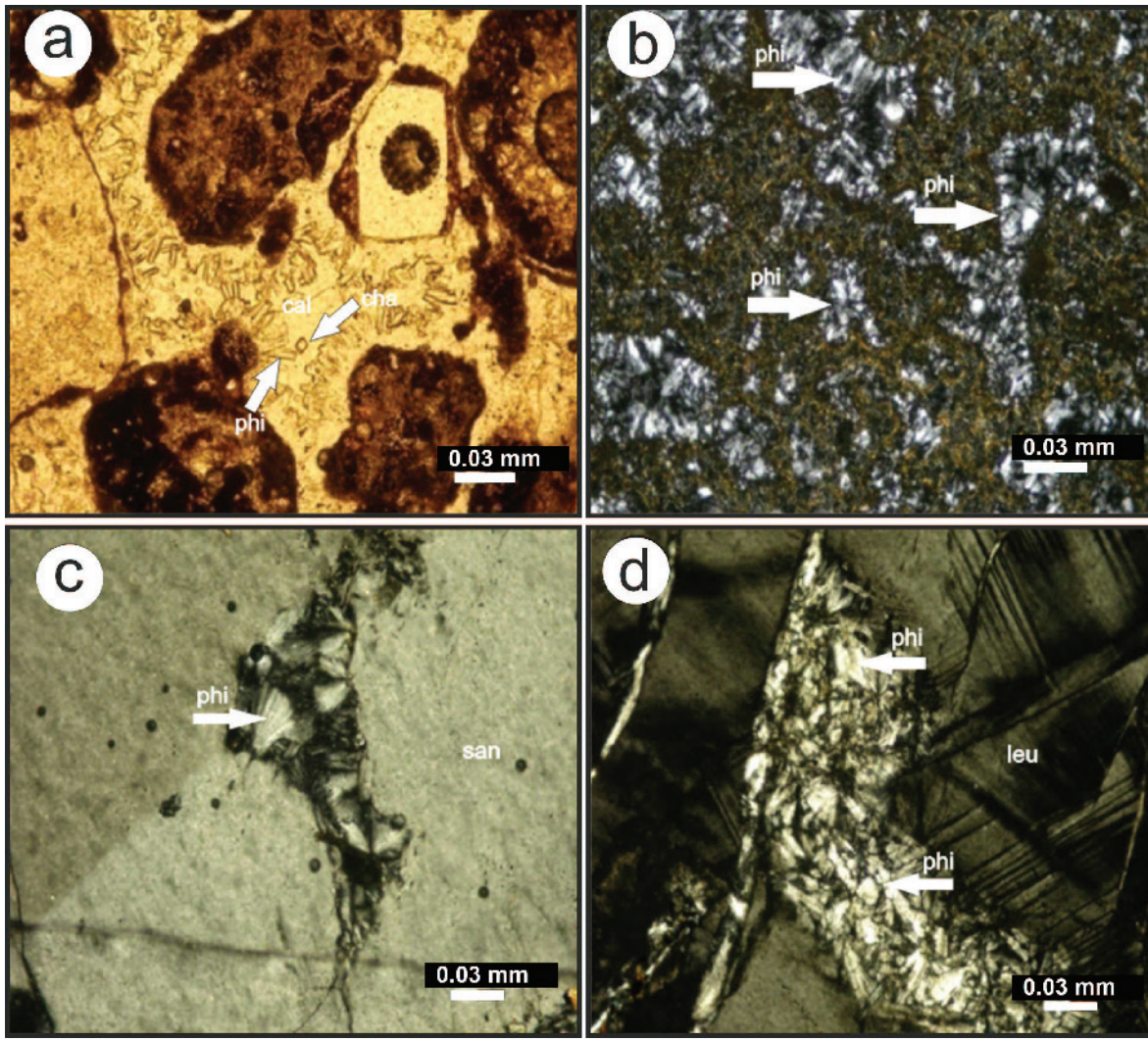

Figure 4. Photomicrographs of characteristic petrographic features of zeolites in HPT from Sandıklı regions: (a) chabazite and phillipsite at the border of pyroclasts from the Ballık area (sample no. B133; PPL); (b) phillipsite in matrix from the Ballık area (sample no. B521; XPL); (c) phillipsite in a crack in sanidine from the Ballık area (sample no. B520; XPL); (d) phillipsite around leucite from the Ömerkuyu area (sample no. O142; XPL). Scale bars shown in mm (cal, calcite; phi, phillipsite; cha, chabazite; leu, leucite; san, sanidine).

appear as isolated euhedral and colorless polygonal crystals. The EDX data for analcime show large Na contents (Figure 7c).

Electron Microprobe (EMPA) backscatter electron images suggest a paragenetic sequence whereby phillipsite crystals grew from the leucite and sanidine (Figure 8a,b; Table 2). Elemental analysis by wavelength dispersive spectroscopy (WDS) of zeolite aggregates (Table 3) were recalculated to structural formulae on the basis of 32 and 24 oxygens for phillipsite and chabazite, respectively. The low totals are due to the presence of structural water. The stoichiometric Si/Al ratio of phillipsites in HPT ranges from 1.99 to 2.62 (Table 3), with small Na contents (<0.1 a.p.f.u.) and large Ca and K contents (0.8−1.4 and 1.3−1.6 a.p.f.u.), respectively. The stoichiometric Si/Al ratios in HPT resemble those of the phonolitic tuffs in the Germany Laach volcanic area, which have been characterized by abundant K and Ca and small Si/Al ratios of 2.33−2.72 (Bernhard and Barth-Wirsching, 2002). The EMPA of chabazite samples in the LPT and HPT showed relatively large SrO contents, which range from 0.46 to 0.79 wt.%. The composition of the chabazite appears to be closely related to the original host-rock composition. The Si/Al ratios of chabazite range from 1.89 to 2.21 (Table 3), which is slightly lower than the phillipsite-rich sample. The Si/Al ratio of chabazite in the tephriphonolitic tuffs of study area also resemble those in the phonolitic tuffs in the Laach volcanic area though they are more abundant in K and Ca and have Si/Al ratios that range

https://doi.org/10.1346/CCMN.2013.0610302 Published online by Cambridge University Press

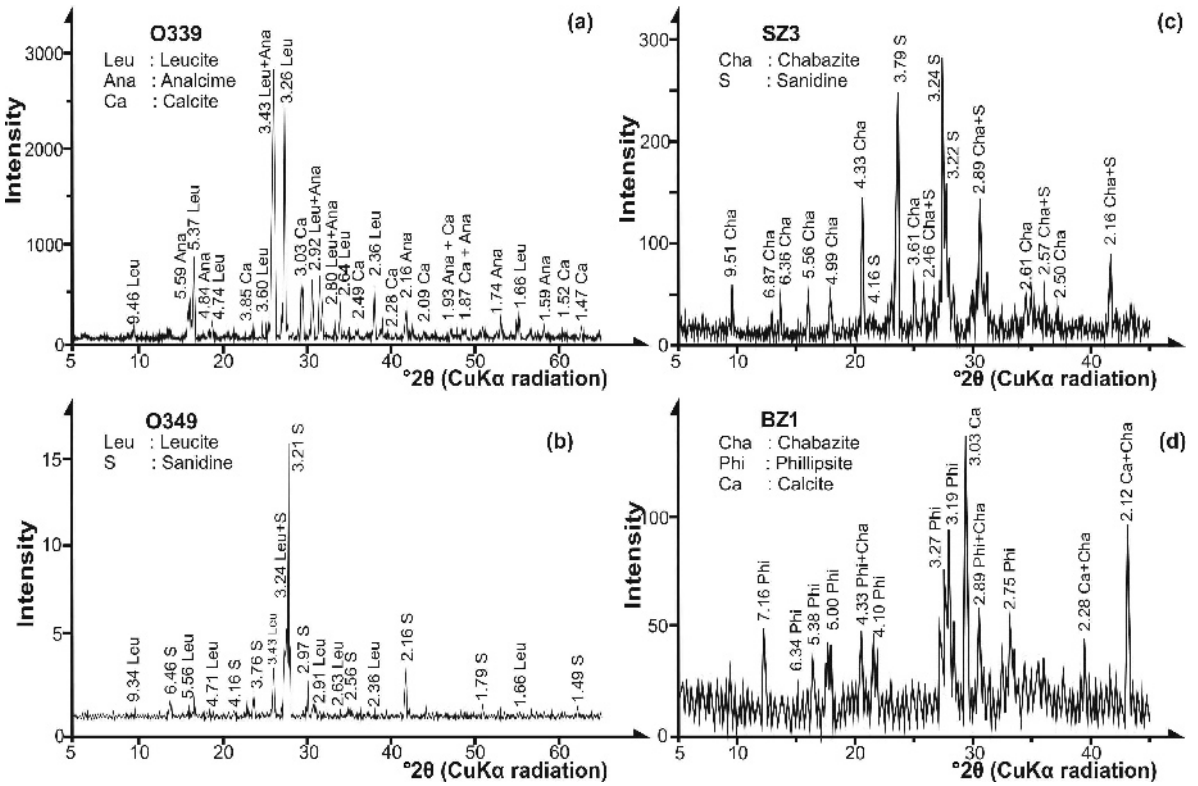

Figure 5. XRD patterns of handpicked leucite crystals and purified zeolite samples: (a) HPT (sample no. O339 from the Soğucak area); (b) HPL specimen including an abundance of sanidine and fewer leucite crystals (sample no. O349 from the Soğucak area); (c) purified zeolite from Selçik area (sample no. SZ3); (d) purified zeolite from the Ballık area (sample No BZ1).

from 2.33 to 2.50 (Bernhard and Barth-Wirsching, 2002).

A triangular plot of (Mg+Ca+Sr), Na, and K (Figure 9a) allows for comparison with other zeolitic terrains (de'Gennaro *et al.*, 2000; Weisenberger and Spürgın, 2009). Zeolites in the present study plot mostly as K-phillipsite ($K_{1.58}Na_{0.10}Ca_{1.33}Al_{5.26}Si_{10.87}O_{32}\cdot 12.90H_2O$) and rarely Ca-chabazite ($Ca_{1.39}Na_{0.06}K_{0.51}Al_{4.01}Si_{8.00}O_{24}\cdot 23.64H_2O$). The phillipsites are Na-depleted and Ca- and K-enriched (Figure 9a). Phillipsites plot near the middle of the K-(Ca+Mg+Sr) line. Chabazites plot closer to the (Ca+Mg+Sr) line. When recast as (Na+K)/(K+Na+Ca+Ba) *vs.* Si/Al (Figure 9b), samples fall in the phillipsite–chabazite field of Chipera and Apps (2001) (see their figure 3). Phillipsites from volcanic rocks have low Si/Al ratios, which are similar to mafic igneous rocks. Phillipsites from deep-sea sediments and saline lake deposits have larger Si/Al ratios and more first-group alkali cations (Sheppard *et al.*, 1970; Oba and Yoshikawa, 1994).

Bulk geochemistry

Representative bulk-chemical analyses of lavas and tuffs from this study are given in Table 4. The samples are classified as trachyte and trachyandesite (HPL, LPT, and HPT) on a Zr/TiO_2 *vs.* Nb/Y diagram like that proposed by Winchester and Floyd (1977) (Figure 10a). Lavas and tuffs were also plotted on a K_2O *vs.* Na_2O diagram (Figure 10b) and show their potassic character, which falls around the dashed line between ultrapotassic and shoshonitic fields. The HPT show high potassic character and fall into the ultrapotassic area of Figure 10b. The LPT show shoshonitic characteristics.

Trachytic and phonolitic rocks have intermediate silica contents and a high percentage of alkali cations (Na^+ and K^+). High proportions of alkali cations indicate that highly alkaline (*i.e.* high pH) pore waters occurred in the tuff vesicles. Under alkaline conditions, the mechanism of zeolite genesis is influenced by excess Si and Al, elements which are rapidly dissolved from volcanic glass and provide the main constituents of zeolites (Hernandez *et al.*, 1993). A similar case is seen in the pyroclastic rocks of Campi Flegrei (southern Italy), which have a narrower range of Si/Al compositions, between 2.59 and 2.86 (*i.e.* from trachyte to phonolite), greater K and Na contents, and moderate concentrations of alkaline earth cations (de' Gennaro *et al.*, 1999). The compositions of pyroclastic rocks of the Sandıklı district vary with broader Si/Al ratios of between 2.49 and 2.99, more K ranging between 2.72 and 7.79, and larger Na contents ranging between 0.40 and 2.12. The secondary minerals in the Sandıklı district are relatively silica poor and

https://doi.org/10.1346/CCMN.2013.0610302 Published online by Cambridge University Press

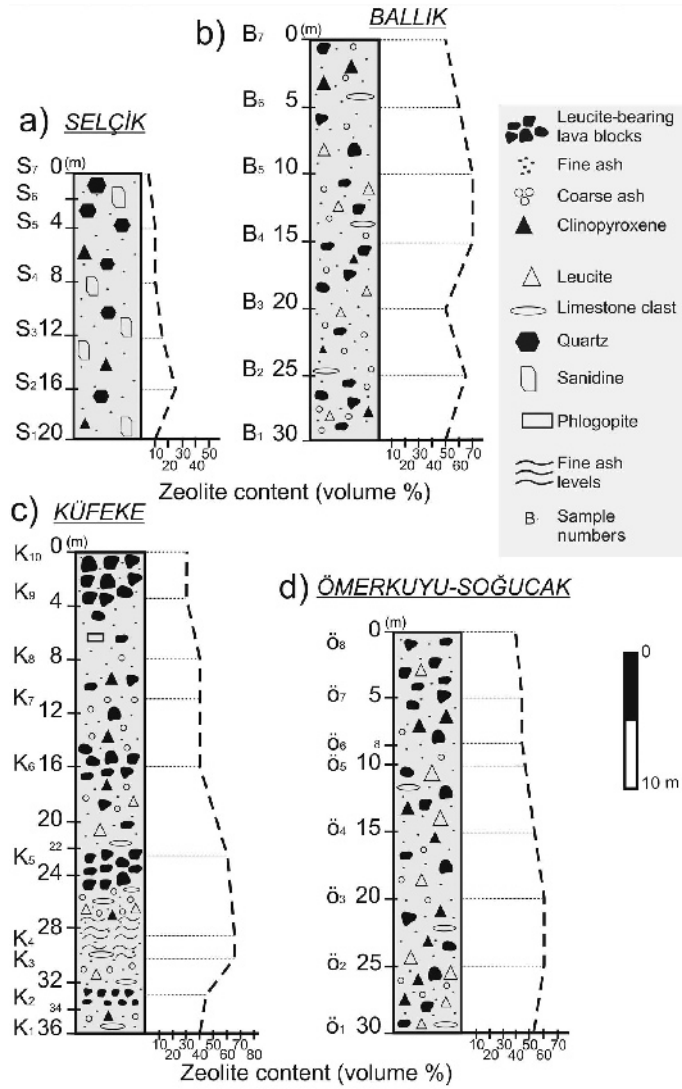

Figure 6. Zeolite contents from lower to upper levels in tuffs of the study area: (a) LPT containing chabazite (Selçik area); (b) HPT containing chabazite and phillipsite (Ballık area); (c) HPT containing phillipsite (Küfeke area); (d) HPT containing phillipsite (Ömerkuyu area). The zeolite content is defined as the mass recovered from heavy liquid separation.

consist mostly of phillipsite and chabazite that formed in K- and Na-rich environments.

DISCUSSION

Controls on zeolitization of pyroclastic rocks

Zeolitization of the pyroclastic deposits of the Sandıklı district was found within two main lithologic units. Chabazite is the dominant zeolite mineral in LPT and both chabazite and phillipsite are dominant in HPT. Zeolitization in the pyroclastic deposits of the Sandıklı district was controlled by processes that depend on: (1) the chemical composition of the source rocks; (2) the deposit thickness and degree of lithification; (3) emplacement temperatures; (4) eruptive dynamics and depositional mechanism and chilling rates; (5) extent of post-depositional meteoric flushing experienced (*i.e.* climatic regime); and (6) the chemistry of the basin sediments into which the deposits accumulated (*i.e.* freshwater *vs.* marine *vs.* hyper-alkaline).

A general summary of the main features of the controls on zeolitization of pyroclastic rocks is given in Table 5. The depositional characteristics of LPT developed from ash-fall deposits while the HPT developed from ash-flow deposits. De'Gennaro *et al.* (2000) suggested that fall processes promoted an effective gas-phase separation and clast dispersion in the atmosphere. In contrast, during flow deposition the steam was retained during the prior transport. When the steam condensed during flow transport the steam was retained and the resulting deposits are relatively wetter and cooler than ash-fall deposits. Both the abundance and

https://doi.org/10.1346/CCMN.2013.0610302 Published online by Cambridge University Press

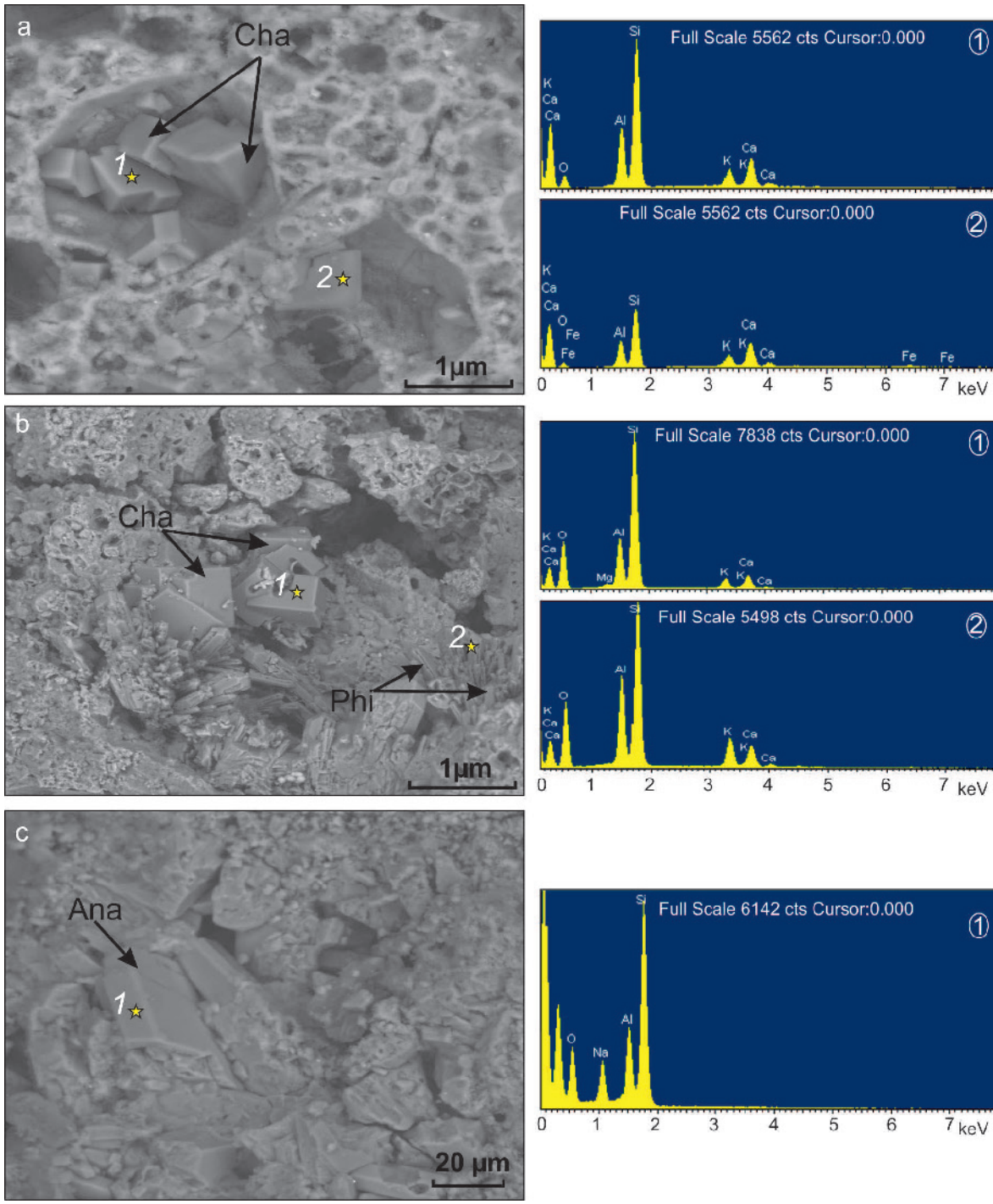

Figure 7. SEM images (left) and the corresponding EDX spectrum (right) of zeolite occurrences in the Sandıklı regions: (a) rhombohedral chabazite crystals formed in cavities from the Ballık area (sample no. B303); (b) rhombohedral chabazite crystals associated with spherulitic radiating prismatic phillipsite crystals from the Soğucak area (sample no. O313); (c) isolated euhedral analcime crystals (sample no. K339). (Arrows indicate examples of different minerals. Stars indicate EDX spectrum points.)

out-fluxing mechanisms of volatile phases in moving pyroclastic flows depend on the initial magma properties and eruptive conditions. Degassing and the cooling processes of a pyroclastic deposit further depend on the initial emplacement conditions, such as deposit thickness. The thickness and porosity of pyroclastic deposits

https://doi.org/10.1346/CCMN.2013.0610302 Published online by Cambridge University Press

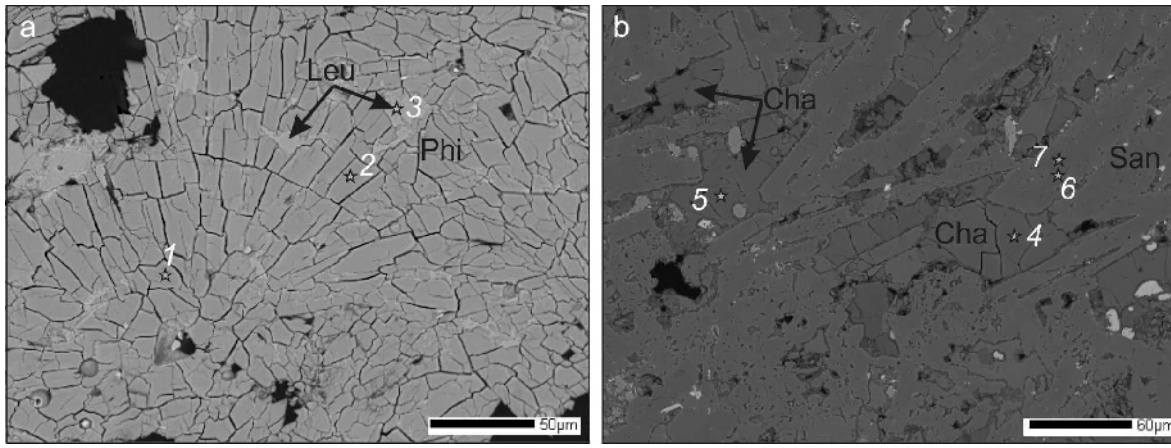

Figure 8. BSE images of chabazite and phillipsite occurrences in the Sandıklı regions: (a) Radiating clusters of phillipsite crystals in the leucite mineral from the Ballık area (sample no. B522); (b) chabazite crystals in sanidine from the Ballık area (sample no. B718). (Analysis numbers (1−7) are the same as those in Table 3. Arrows indicate examples of different minerals.)

decrease with time due to volatile out-fluxing, compaction, and welding. The Sandıklı pyroclastic succession ranges between 20 and 50 m thick. The lithification processes began by the formation of zeolites (mainly chabazite and phillipsite) and in the case of Sandıklı, the extent of lithification in LPT is less than that of HPT. The thicknesses and emplacement temperatures of pyroclastic rocks were lower in the LPT. The LPT was formed as an ash-fall deposit that did not entirely fill the pre-existing deepest valley. Hence the emplacement

Table 2. Microprobe analyses of K-phillipsite and leucite (sample no. B522) and Ca-chabazite and sanidine (sample no. B718) of the Sandıklı volcanics.

Sample No	B522			B718			
	– K-Phillipsite –		Leucite	Ca-Chabazite		– Sanidine –	
Analysis no.	1	2	3	4	5	6	7
SiO_2	53.15	51.15	55.60	38.47	43.80	63.86	65.00
TiO_2	0.25	0.34	0.07	0.07	0.01	0.04	0.07
Al_2O_3	23.02	20.59	22.77	23.03	18.88	19.79	19.04
MgO	0.07	0.10	0.00	0.06	0.01	0.00	0.00
FeOt	0.30	0.17	0.64	0.15	0.02	0.51	0.73
MnO	0.00	0.13	0.08	0.08	0.08	0.21	0.08
CaO	6.34	6.26	0.04	8.95	9.76	1.29	0.15
K_2O	5.66	6.17	20.17	2.92	2.22	9.72	13.27
Na_2O	0.18	0.22	0.10	0.05	0.10	3.38	1.96
BaO	1.14	0.57	0.24	0.63	0.64	0.07	0.13
SrO	0.38	0.31	0.20	0.93	0.84	n.d.	n.d.
Total	90.48	86.01	99.91	75.33	76.37	99.49	100.78
Σ cations:	– 32 oxygens –		6 oxygens	– 24 oxygens –		— 8 oxygens —	
Si	10.700	10.849	2.017	7.085	7.856	2.932	2.971
Ti	0.037	0.054	0.002	0.009	0.002	0.001	0.002
Al	5.462	5.147	0.974	4.999	3.991	1.071	1.026
Mg	0.020	0.032	0.000	0.016	0.002	0.000	0.000
Fe	0.051	0.030	0.019	0.023	0.003	0.020	0.028
Mn	0.000	0.023	0.002	0.012	0.012	0.008	0.003
Ca	1.368	1.423	0.002	1.766	1.876	0.063	0.008
K	1.453	1.669	0.933	0.687	0.509	0.569	0.774
Na	0.070	0.090	0.007	0.017	0.035	0.301	0.174
Ba	0.090	0.048	0.003	0.045	0.045	0.001	0.002
Sr	0.044	0.038	0.004	0.099	0.087	n.d.	n.d.
Total	19.294	19.403	3.964	14.759	14.418	4.966	4.988

n.d. not detected.

https://doi.org/10.1346/CCMN.2013.0610302 Published online by Cambridge University Press

Table 3. Representative electron microprobe analyses [mean values; ( ): number of analyses used] of phillipsite and chabazite from the zeolitic tuffs of the Sandıklı area.

Mineral sample no.	MDL	– Chabazite –		Phillipsite					
		B718 (4)	K334 (3)	B718 (2)	B718 (2)	B518 (6)	B518 (5)	B522 (2)	B522 (1)
	wt.%	wt.%	wt.%	wt.%	wt.%	wt.%	wt.%	wt.%	wt.%
SiO_2	0.0856	44.69	47.52	57.05	51.91	51.12	51.31	52.15	51.26
TiO_2	0.1020	0.12	0.18	n.d.	0.11	0.10	n.d.	0.29	0.10
Al_2O_3	0.0796	20.25	18.53	18.49	21.68	21.63	21.92	21.81	20.78
FeO	0.3152	0.17	0.63	n.d.	0.45	0.33	0.26	0.24	n.d.
MnO	0.2739	n.d.	n.d.	n.d.	n.d.	n.d.	n.d.	n.d.	n.d.
MgO	0.0902	n.d.	0.88	n.d.	n.d.	n.d.	n.d.	0.08	0.12
CaO	0.0618	8.99	5.41	3.79	6.34	6.12	6.26	6.30	5.69
Na_2O	0.1185	0.22	0.12	0.43	0.13	0.25	0.19	0.20	0.30
K_2O	0.0608	2.37	2.23	5.00	5.98	6.09	6.07	5.92	5.76
BaO	0.2178	0.55	0.27	2.41	1.12	0.75	0.71	0.86	0.85
SrO	0.1458	0.79	0.46	0.26	0.25	0.22	0.23	0.34	0.19
Total		76.45	76.24	87.49	88.03	86.66	87.05	88.25	85.16
Si		7.778	8.288	11.731	10.781	10.759	10.728	10.774	10.922
Al		4.179	3.807	4.482	5.307	5.362	5.420	5.305	5.219
Ti		0.015	0.024	0.000	0.017	0.015	0.007	0.046	0.017
Fe		0.025	0.093	0.009	0.078	0.059	0.046	0.040	0.000
Mn		0.006	0.000	0.000	0.002	0.004	0.007	0.012	0.019
Mg		0.011	0.228	0.002	0.013	0.011	0.006	0.026	0.037
Ca		1.685	1.011	0.835	1.411	1.380	1.407	1.395	1.299
Na		0.072	0.041	0.171	0.053	0.100	0.077	0.080	0.125
K		0.530	0.496	1.313	1.584	1.634	1.623	1.561	1.565
Ba		0.038	0.019	0.194	0.091	0.062	0.059	0.069	0.071
Sr		0.080	0.047	0.031	0.030	0.027	0.028	0.041	0.023
Oxygens =		24	24	32	32	32	32	32	32
Ca+Mg		1.696	1.240	0.837	1.424	1.391	1.413	1.421	1.336
Na		0.072	0.041	0.171	0.053	0.100	0.077	0.080	0.125
K		0.530	0.496	1.313	1.584	1.634	1.623	1.561	1.565
Si/Al		1.893	2.208	2.617	2.032	2.020	1.994	2.033	2.093
(K+Na)/K+Na+Ca)		0.264	0.341	0.639	0.537	0.557	0.547	0.540	0.565
Tsi=Si/(Si+Al)		0.651	0.685	0.724	0.670	0.667	0.664	0.670	0.677

MDL, minimum detection limit; n.d. not detected

temperature reduced more quickly and resulted in smaller zeolite contents and less lithification. The absence of columnar jointed blocks in both LPT and HPT suggests that the emplacement temperature was not high (Francis *et al.*, 1974). The degree of lithification in the lower and middle sections of both LPT and HPT were noted (Özpınar *et al.*, 2002) to have been greater than in the upper levels. The LPT have average porosity of 31% and a compressive strength of 9 Mpa. In contrast, HPT (with chabazite and phillipsite) have a similar average porosity of 29%, but much higher compressive strengths of up to 18 Mpa. The HPT, dominated by phillipsite alone, have a similar average porosity of 28% and compressive strengths of up to 18 Mpa.

In a closed hydrologic system where the basin was without effluent streams, a saline alkaline lake typically formed at its center (Gottardi, 1989). Geomorphological conditions support the migration of both surface and pore waters toward the deepest part of the basin. Evaporation plays an important role in modifying the composition of water that eventually becomes connate. Concentric zoning of waters resulting from evaporation and shrinkage of the water-filled portion of the basin is reflected in the patterns of authigenic mineral deposits. What appears is progressive formation of an outer and upper ring of fresh or altered glass, an intermediate ring with zeolites, and a final central ring with alkali feldspar (Langella *et al.*, 2001). In contrast to open hydrologic systems that have meteoric waters percolating slowly through the thick tuff layers, the compositions of closed systems change progressively and become more alkaline and saline (and higher in pH). As the water descends near the surface, the glass is altered to clay minerals; a little deeper it alters to zeolite (chabazite and phillipsite); more deeply still it alters to analcime; and at the lowest level it alters to alkali feldspar (Gottardi, 1989; Sheppard and Hay, 2001).

In both the LPT and HPT from Sandıklı, concentric zoning of authigenic minerals was not seen. The zeolitization shows much less distinctive vertical

https://doi.org/10.1346/CCMN.2013.0610302 Published online by Cambridge University Press

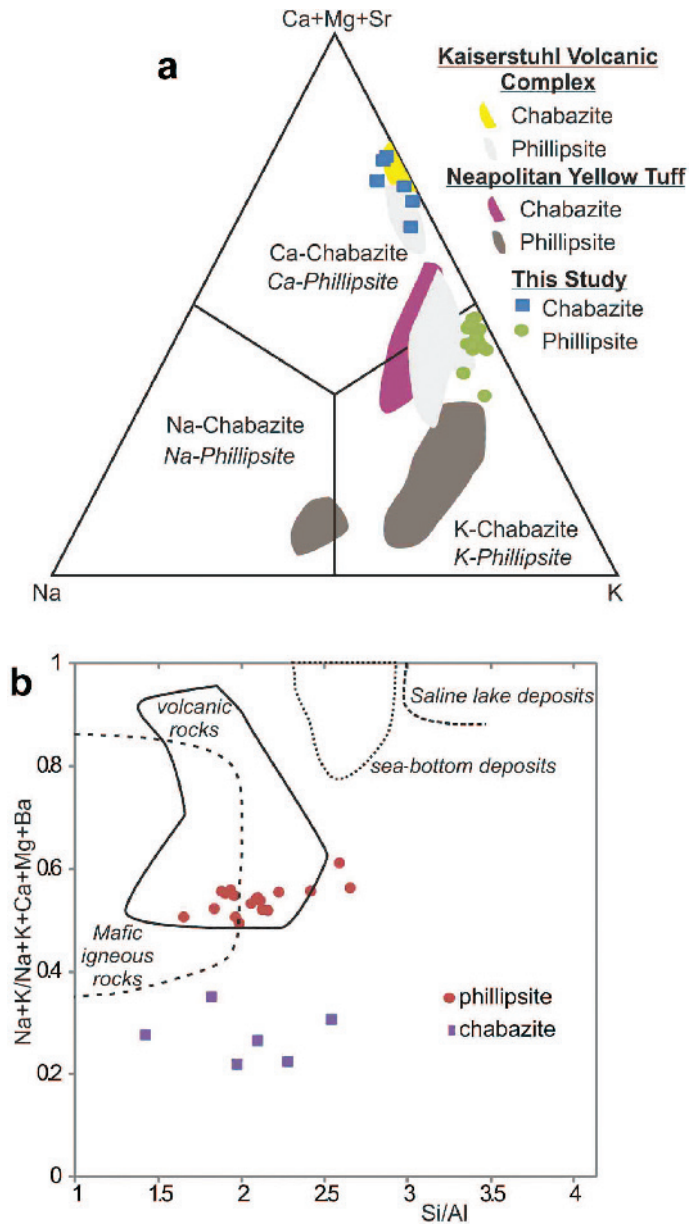

Figure 9. (a) Zeolite compositions from microprobe analyses plotted on a ternary Na-K-(Ca+Mg+Sr) composition diagram. The bounded areas are from de'Gennaro *et al.* (2000) and Weisenberger and Spürgın (2009); (b) plot showing the proportion of (Na+K)/(K+Na+Ca+Mg+Ba) *vs.* the Si/Al ratios of the investigated area. The bounded areas represent compositional fields for phillipsites from Oba and Yoshikawa (1994). Samples B718, B518, B522, and S335 are pyroclastic rocks from the areas of Ballık (samples B718, B518, and B522) and Selçik (sample S335 only).

zonation than seen in other areas (Table 5). Authigenic K-feldspar (sanidine) was not observed. Sanidine seen in thin section and observed with XRD is related to the original pyroclasts and pyrogene mineralization within tuffs. Back-scattered electron images showing chabazite transformed from primary sanidine (Figure 8b) further support this notion. The lack of evaporite minerals in the study area is also an indicator of an open hydrologic system. When combined, the Upper Jurassic–Lower Cretaceous permeable limestone Akdağ Formation underlying the pyroclastic rocks enhanced the alkaline nature of the subsurface environment while at the same time produced a conduit for water to migrate away.

The occurrence of analcime formation based on experimental studies is explained as coming from a primary magmatic source (*i.e.* formation from a fluid phase) and from a secondary transformation of leucite to analcime. Primary formation produces aggregates of well formed crystals with smooth surfaces, while secondary formation produces a micron-sized

https://doi.org/10.1346/CCMN.2013.0610302 Published online by Cambridge University Press

Table 4. Major (wt.%), trace (ppm), and rare-earth element (ppm) compositions of the Sandıklı volcanics.

	Lavas								Tuffs						
	O314	O310	S110	S126	S132	O141	K200	S824	B303	O311	O321	O331	S338	S811	S817
SiO_2	54.02	51.13	61.19	59.91	61.79	50.88	59.69	62.29	47.80	48.07	45.90	56.36	54.05	54.49	50.32
Al_2O_3	17.15	16.94	14.84	15.51	14.68	17.14	14.6	14.54	16.32	16.99	14.67	18.02	16.12	16.06	17.49
Fe_2O_3	4.43	5.62	4.93	5.46	5.50	7.07	5.15	4.80	4.97	5.23	7.72	3.80	3.90	3.55	5.40
MgO	1.51	2.13	2.49	2.64	2.15	1.36	2.94	3.03	0.92	0.84	2.72	0.46	1.09	1.30	1.17
CaO	5.10	6.54	4.53	4.48	3.97	6.19	4.35	3.95	4.90	4.96	6.78	3.49	4.92	4.12	3.24
Na_2O	1.53	1.85	3.12	3.57	2.86	2.49	2.35	3.33	0.55	0.54	0.32	2.86	2.17	1.92	0.69
K_2O	10.12	7.73	4.87	4.51	5.03	8.10	4.85	5.09	6.04	7.33	7.90	7.73	3.69	3.28	9.31
TiO_2	0.74	0.86	1.04	1.09	0.92	1.29	1.10	0.99	0.84	0.91	1.26	0.66	0.57	0.65	0.97
P_2O_5	0.33	0.45	0.66	0.53	0.63	0.21	0.77	0.59	0.14	0.22	0.51	0.09	0.25	0.30	0.19
MnO	0.09	0.10	0.10	0.19	0.10	0.13	0.07	0.09	0.09	0.09	0.15	0.10	0.08	0.07	0.09
Cr_2O_3	0.006	0.006	0.015	0.02	0.015	0.004	0.01	0.026	n.d	0.002	0.006	n.d	0.004	0.09	0.06
LOI	4.1	5.6	1.8	1.5	2.0	3.8	3.4	0.8	16.2	13.7	10.9	5.3	12.2	13.3	10.3
Total	99.14	98.93	99.62	99.54	99.67	98.74	99.61	99.52	98.80	98.90	98.83	98.87	99.05	99.30	99.23
Pb	36.5	33.7	5.0	16.0	6.0	75.0	7.0	9.0	58.6	60.4	74.0	5.8	34.6	32.0	62.0
Zn	41	50	32	62	29	42	47	39	65	63	67	27	58	59	78
Ni	6.8	8.4	21.0	22.0	24.0	<20	22.0	25.0	3.6	6.1	10.6	4.7	12.1	23.0	19.0
Ba	2545	3397	1756	2000	1961	5582	1856	1687	4392	4862	6095	2217	4636	3797	4421
Co	16.9	16.2	16.9	18.3	20.1	17.8	17.1	17.2	10.2	12.0	22.4	13.8	10.0	9.6	9.4
Hf	17.4	27.3	13.1	9.8	11.0	21.4	15.4	12.3	16.8	16.9	17.0	15.9	9.8	10.4	15.8
Nb	33.9	34	45.5	40.7	32.6	52.5	47.6	43.4	41.2	41.7	36.8	36.9	42.7	57.1	41.6
Rb	638.8	1042	180.8	161.1	292.9	1776	194.6	216.4	381.1	415.6	351.4	248	156.7	167.5	393.2
Sr	2910	3460	1208	1452	1020	3246	1320	1237	4287	2615	1786	5783	2094	1954	1552
Ta	1.9	1.7	3.3	3.2	3.0	3.7	3.8	3.9	2.2	2.4	2.0	2.5	2.3	3.3	2.8
Th	49.4	46.7	29.8	45.0	53.4	54.5	34.0	40.1	49.1	47.6	45.8	41.3	45.7	47.9	43.9
V	121.0	153.0	92.0	11.4	127.0	216.0	11.0	81.0	88.0	154.0	155.0	74.0	61.0	61.0	132.0
W	53.5	20.9	6.0	4.0	7.0	4.0	8.0	5.0	7.5	8.1	9.7	64.1	18.7	6.0	3.0
Zr	655.4	630.3	457.8	327.6	343.7	774	520.4	419.9	640.4	636.8	597.1	593.2	389.8	419.2	517.9
Y	21.1	19.3	26.7	26.3	28.6	28.3	31.2	25.0	20.0	28.5	24.3	22.7	19.2	30.0	23.0
La	74.4	84.3	103.8	135.0	76.7	104.7	121.7	103.3	76.4	94.6	81.2	79.2	124.0	147.9	85.5
Ce	135.3	142.1	184.5	239.7	129.9	179.3	219.8	186.1	143.3	164.5	160.4	135.2	214.1	222.4	142.7
Pr	13.8	16.1	20.2	26.39	14.74	19.74	24.5	20.45	14.58	17.66	17.56	14.44	19.52	21.85	15.14
Nd	50.2	59.0	73.5	97.6	56.6	69.4	88.4	72.3	49.4	64.5	64.0	53.3	62.9	71.9	54.0
Sm	7.40	8.90	12.00	15.20	9.40	12.10	14.60	11.20	7.65	9.36	10.83	7.79	8.11	9.80	8.60
Eu	1.87	2.16	3.35	4.15	2.39	3.10	4.10	3.10	1.89	2.33	2.59	1.95	1.90	2.53	1.19
Gd	5.07	5.88	7.6	8.76	6.88	7.92	9.76	7.35	5.11	6.45	7.37	5.53	5.25	6.045	5.53
Tb	0.73	0.81	0.9	1.01	0.86	1.00	1.13	0.9	0.77	0.91	1.00	0.77	0.68	0.73	0.70
Dy	3.74	3.71	4.71	5.10	4.85	5.15	5.73	4.56	3.66	4.35	4.71	4.00	3.26	4.15	3.81
Ho	0.68	0.61	0.88	0.87	0.94	0.93	1.01	0.70	0.68	0.78	0.82	0.70	0.60	0.86	0.69
Er	1.92	1.81	2.58	2.52	3.01	2.8	2.99	2.32	1.96	2.14	2.16	2.02	1.74	2.77	2.24
Tm	0.30	0.26	0.33	0.32	0.38	0.37	0.39	0.30	0.30	0.33	0.32	0.30	0.26	0.38	0.29
Yb	1.97	1.78	2.30	2.24	2.69	2.53	2.7	2.13	1.92	2.14	2.04	1.99	1.74	2.82	2.02
Lu	0.31	0.27	0.33	0.30	0.39	0.35	0.35	0.31	0.28	0.30	0.29	0.31	0.26	0.44	0.28

microporous texture (Putnis *et al*., 1994; Line *et al*., 1995; Abdioğlu, 2012) showing the typical leucite habit of deltoid-icositetrahedron with well developed {211} faces. A proposed reaction is leucite + Na^+_{aq} + H_2O = analcime + K^+_{aq}, which involves a 10% molar-volume increase that produces the cracking around the analcime aggregate (Putnis *et al.*, 2007; Weisenberger and Spürgın, 2009). Laboratory simulations using this reaction path suggest that analcime is the most stable phase, often resulting from metastable phillipsite and chabazite (de'Gennaro *et al.*, 2000). In the Sandıklı area, the transformation of leucite into analcime probably occurred under neutral to moderately alkaline conditions after the deposition of the tuffs. X-ray diffraction analysis shows leucite in glass and volcanic rock fragments (volcanic clasts) within HPT.

The formation of phillipsite and chabazite requires K, whereas Ca is less important in most zeolite crystallization in trachytic-phonolitic glasses. Unlike other zeolite occurrences around the world, the chabazite in both LPT and HPT are Ca-enriched which probably occurred by both direct formation in Ca-bearing solutions and by post-zeolitization cation exchange. The concentration of K or the K/(Ca+Na) ratio needs to be sufficiently high to precipitate phillipsite at the initial stage of zeolitization. At Sandıklı, the concentration of

https://doi.org/10.1346/CCMN.2013.0610302 Published online by Cambridge University Press

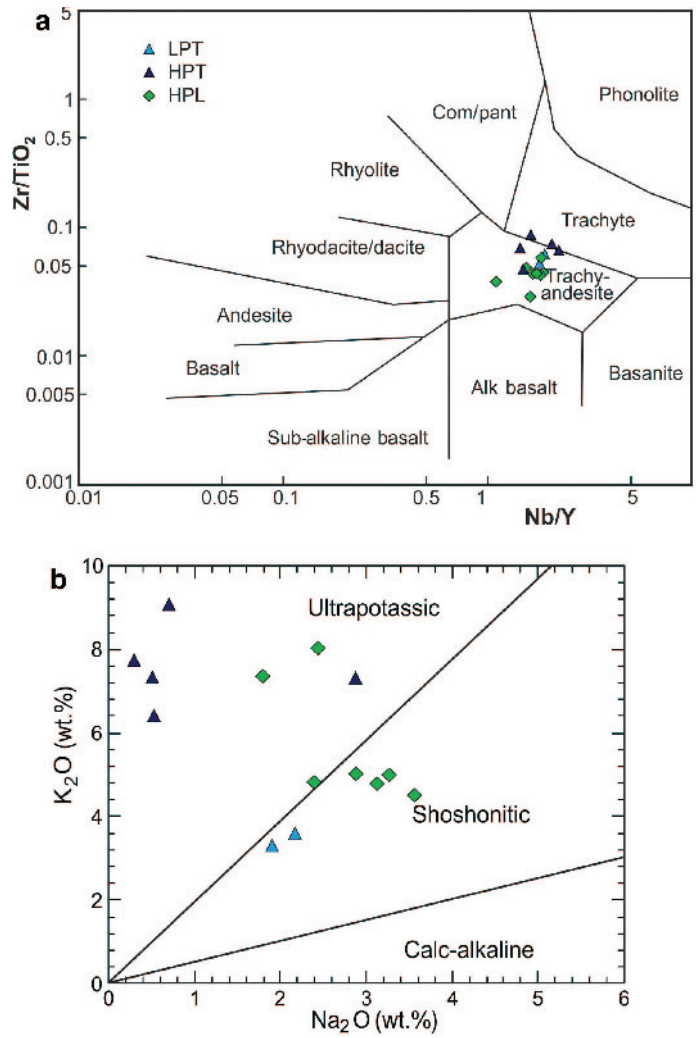

Figure 10. (a) Zr/TiO_2 *vs*. Nb/Y chemical classification diagram for lavas and tuffs from the study area. (b) K_2O *vs.* Na_2O diagram for lavas and tuffs. Stars are tuffs (LPT, HPT) and squares are volcanics/lavas (PL, PAL, HPL).

Na appears to have increased downward as the excess Na was derived from glass dissolution with percolating water through porous tuffs. As the K/(Ca+Na) decreases with phillipsite precipitation, the chabazite begins to crystallize (Iıjima and Harada, 1969). Increasing the fugacity of CO_2 can further influence the formation of zeolites by lowering the activity of H_2O and by providing the carbonate ions by hydrolysis reactions. Carbonate ions can combine with Ca to form calcite, thus creating a Ca sink, which otherwise is used in forming Ca zeolites (Hay, 1986; İbrahim, 2004). The absence of calcite and enrichment of Ca, therefore, suggests lower CO_2 fugacity during zeolitization.

The order of paragenesis of the authigenic minerals in the zeolitization in the pyroclastic deposits is indicated as [analcime/phillipsite → chabazite → calcite]. Analcime/phillipsite was not found together with chabazite in LPT. Analcime appears along with minor calcite only in the Ballık and Soğucak areas.

CONCLUSIONS

Field, petrographic, and petrochemical investigations performed to understand the conditions of formation of the Sandıklı zeolite deposits revealed two different lithologic units: LPT and HPT. The parent materials of these units have been transformed to zeolite minerals by percolating meteoric water, probably in an open hydrological system. The LPT are shoshonitic in character and Ca-chabazite formed as a result. The HPT are more highly potassic in character and characterized by the predominance of K-phillipsite and lesser amounts of Ca-chabazite and analcime. The zeolite contents of the middle and lower sections (both of LPT and HPT) are more abundant than in the upper sections, with zeolite contents for the LPT of as much as 25% and 70% for HPT. These deposits are slightly more potassic and more calcic in composition than typical zeolitic deposits derived from volcanic tuffs in other regions of the world. Exploration and exploitation of zeolitic deposits

https://doi.org/10.1346/CCMN.2013.0610302 Published online by Cambridge University Press

Table 5. Comparison of zeolite assemblages.

Zeolitization factors	Sandıklı	Italy[1]	Spain[2]	Germany[3]	Turkey[4]
Source rock	Trachyte, tephriphonolite	Trachyte and phonolite	Trachytic and phonolitic rocks	Phonolite	Basaltic rocks
Zeolite type	Phillipsite, chabazite, minor analcime	Phillipsite, minor chabazite	Phillipsite with lesser chabazite and analcime	Chabazite, phillipsite and analcime	Natrolite, analcime, disordered thomsonite, laumontite and phillipsite
Deposit thickness (m)	20–50	20–30	–	0.15–10	–
Emplacement temperature (ºC)	Not high	Not lower than 375	Lower	100–200	100
Eruptive dynamics and mechanisms	Ash-flow and ash-fall deposits	Pyroclastic-flow and minor air-fall deposits	Ash flows and rare ash falls	Pyroclastic ash flow	Brecciated lavas, tuff-lapilli tuff
Meteoric flushing	Meteoric waters	Meteoric waters	Water vapor trapped within the pores of the glass particles	Stagnant fringe water zone immediately above the groundwater table	Mixture of seawater and meteoric water with magmatic water
Open or closed system conditions	Open hydrologic system	Alteration in an open hydrologic system	Closely related to the hydro-thermal system	Relatively closed system	Closed system

[1]de' Gennaro *et al*. (2000); [2]Hernandez *et al*. (1993); [3]Bernard and Barth-Wirsching (2002); [4]Abdioglu (2012).

hosting analcime, chabazite, and phillipsite might consider using the factors of magmatic source-rock composition, temperature/cooling history, emplacement mechanism, and deposit thickness in development strategies.

ACKNOWLEDGMENTS

The authors extend thanks to Jianguo Fan (Center for Advanced Ultrastructural Research, University of Georgia) for his help with the scanning electron microscopy and Chris Fleshier (Department of Geology, University of Georgia) for his help with the electron microprobe analysis. Murat Kalkan (Aksaray University) is acknowledged for his assistance during the fieldwork. The editorial team and two anonymous reviewers are thanked for their comments which significantly improved the manuscript.

REFERENCES

Abdioğlu, E. (2012) Mineralogy and chemistry of zeolites and associated minerals in Tertiary alkaline volcanics from the Eastern Pontides, NE Turkey. *Neues Jahrbuch für Mineralogie*, **189**, 35–47.

Armstrong, J.T. (1988) Quantitative analysis of silicate and oxide materials: comparison of Monte Carlo, ZAF, and phi-rho-z procedures. *Microbeam Analysis* **23**, 239–246.

Bernhard, F. and Barth-Wirsching, U. (2002) Zeolitization of a phonolitic ash flow by groundwater in the Laach volcanic area, Eifel, Germany. *Clays and Clay Minerals*, **50**, 710–725.

Besang, C., Eckahtrdt, F.J., Harre, W., Kreuzer, H., and Müller, P. (1977) Radiometricshe Altersbesttimmungen der Türkei. *Jahrbuch der Geologischen Bundesanstalt*, **25**, 3–5.

Bish, D.L. and Carey, J.W. (2001) Thermal behavior of natural zeolites. Pp. 403–452 *in: Natural Zeolites: Occurrence, Properties, Applications* (D.L. Bish and D.W. Ming, editors). Reviews in Mineralogy and Geochemistry, **45**, Mineralogical Society of America, Washington, D.C.

Cappelletti, P., Cerri, G., Colella, A., de' Gennaro, M., Langella, A., Perrotta, A., and Scarpati, C. (2003) Post-eruptive processes in the Campanian Ignimbrite. *Mineralogy and Petrology* **79**, 79–97.

Chipera, S.J. and Apps, J.A. (2001) Geochemical stability of natural zeolites. Pp. 117–161 *in: Natural Zeolites: Occurrence, Properties, Applications* (D.L. Bish and D.W. Ming, editors). Reviews in Mineralogy and Geochemistry, **45**, Mineralogical Society of America, Washington D.C.

de'Gennaro, M., Langella, A., Cappelletti, P., and Colella, C. (1999) Hydrothermal conversion of trachytic glass to zeolite. 3. Monocationic Model Glasses. *Clays and Clay Minerals*, **47**, 348–357.

de'Gennaro, M., Cappelletti, P., Alangella, A., Perrotta, A., and Scarpati, C. (2000) Genesis of zeolites in the Neapolitan Yellow Tuff: Geological, volcanological and mineralogical evidence. *Contributions to Mineralogy and Petrology*, **139**, 17–35.

Ercan, T. (1986) Orta Anadolu'daki Senozoyik Volkanizması. *MTA Dergisi*, **107**, 119–141 (in Turkish).

Esenli, F. and Sirkecioglu, A. (2005) The relationship between zeolite (heulandite-clinoptilolite) content and the ammonium-exchange capacity of pyroclastic rocks in Gördes, Turkey. *Clay Minerals*, **40**, 557–564.

Folk, (1962) Classification of carbonate rocks. *American Association of Petroleum Geologists Memoirs*, **1**, 62–82.

Francis, P.W., Roobol, M.J., Walker, G.P.I., Cobbold, P.R. and Coward, M. (1974) The San Pedro and San Pablo Volcanoes and their hot avalanche deposits. *Geologische Rundschau*, **63**, 357–388.

Gottardi, G. (1989) The genesis of zeolites. *European Journal of Mineralogy*, **1**, 479–487.

Gundogdu, M.N., Yalcin, H., Temel, A., and Clauer, N. (1996) Geological, mineralogical and geochemical characteristics of zeolite deposits associated with borates in the Bigadic Emet and Kirka Neogene lacustrine basins, western Turkey. *Mineralium Deposita*, **31**, 492–513.

Hay, R.L. (1986) Geologic occurrence of zeolites and some associated minerals. *Pure and Applied Chemistry*, **58**, 1339–1342.

Helvacı, C., Stamatakis, M.G., Zagouroglou, C., and Kanaris, J. (1993) Borate minerals and related authigenic silicates in northeastern Mediterranean late Miocene continental basins. *Exploration and Mining Geology*, **2**, 171–178.

Hernandez, J.E.G., Notario del Pino, J.S., Gonzalez Martin, M.M., Hernan Reguera, F., and Rodriguez Losada, J.A. (1993) Zeolites in pyroclastic deposits in southeastern Tenerife (Canary Islands). *Clays and Clay Minerals*, **41**, 521–526.

Ibrahim, K. (2004) Mineralogy and chemistry of natrolite from Jordan. *Clay Minerals*, **39**, 47–55.

Iıjima, A. and Harada, K. (1969) Authigenic zeolites in zeolitic palagonite tuffs on Oahu, Hawaii. *American Mineralogist*, **54**, 182–198.

Kaçmaz, H. and Koktürk, U. (2004) Geochemistry and mineralogy of zeolitic tuffs from the Alacatı (Ceşme) area, Turkey. *Clays and Clay Minerals*, **52**, 705–713.

Langella, A., Cappeletti, P., and de'Gennaro, M. (2001) Zeolites in closed hydrologic systems. Pp. 235–260 in: *Natural Zeolites: Occurrence, Properties, Applications* (D.L. Bish and D.W. Ming, editors). Reviews in Mineralogy and Geochemistry, **45**, Mineralogical Society of America, Washington, D.C.

Line, C.M.B., Putnis, A., Putnis, C., and Giampaolo, C. (1995) The dehydration kinetics and microtexture of analcime from two paragenesis. *American Mineralogist*, **80**, 268–279.

Minato, H. (1992) Investigation methods of zeolite, *Natural Zeolite and its Utilization*, Edited By No. 111 Committee, JSPS, Tokyo University Press, Tokyo, pp. 281–376.

Oba, T. and Yoshikawa, K. (1994) Note on rock-forming minerals in the Joetsu district, Niigata Prefecture, Japan. (7) Phillipsite from Yoneyama. *Bulletin Joetsu University of Education*, **13**, 399–406.

Özen, S. and Göncüoğlu, M.C. (2011) Origin of analcime in the Neogene Arıklı tuffs, Biga Peninsula, NW Turkey. *Neues Jahrbuch für Mineralogie*, **189/1**, 21–34.

Özpınar, Y., Çobanoğlu, I., and Bozkurt, R. (2002) Sandıklı zeolitik tüflerin petrografik ve petrokimyasal ve teknolojik özelliklerinin incelenmesi, TÜBİTAK-YDABÇAĞ-198Y102, Ankara, pp 268 (in Turkish).

Özpınar, Y. (2008) The mineralogic, petrographic and ion exchange capacity features of tuffs containing chabazite and phillipsite in Sandıklı (Afyon) region and their usage in agriculture (southwest Anatolia, Turkey). *Bulletin of the Mineral Research and Exploration*, **137**, 29–48.

Özpınar, Y. (2011) Use of zeolitic tuffs as cement additives, building stone and removal of heavy metal cations. *Carpathian Journal of Earth and Environmental Science*, **6/1**, 147–158.

Putnis, A., Putnis, C., and Giampolo, C. (1994) The microtexture of analcime phenocrysts in igneous rocks. *European Journal of Mineralogy*, **6**, 627–632.

Putnis, C.V., Geisler, T., Schmid-Beuermann, P., Stephan, T., and Giampaolo, C. (2007) An experimental study of the replacement of leucite by analcime. *American Mineralogist*, **92**, 19–26

Schmid, R. (1981) Descriptive nomenclature and classification of pyroclastic deposits and fragments: Recommendations of the IUGS Sub-commission on the Systematics of Igneous Rocks. *Geology*, **9**, 41–44.

Semiz, B., Schroeder, P.A., and Özpınar, Y. (2011) Zeolitization of Miocene tuffs the Saphane-Gediz-Hisarcık regions, Kutahya-western Anatolia, (Turkey). *Euroclay 2011*, Antalya, Turkey, 232 pp.

Sheppard, R.A. and Hay, R.L. (2001). Formation of zeolites in open hydrologic systems. Pp. 261–271 in: *Natural Zeolites: Occurrence, Properties, Applications* (D.L. Bish and D.W. Ming, editors). Reviews in Mineralogy and Geochemistry, **45**, Mineralogical Society of America, Washington, D.C.

Sheppard, R.A., Gude, A.J. 3rd, and Griffin, J.J. (1970) Chemical composition and physical properties of phillipsite from the Pacific and Indian Oceans. *American Mineralogist*, **55**, 2053–2062.

Snellings, R., van Haten, T., Machiels, L., Mertens, G., Vandenberghe, N., and Elsen, J. (2008) Mineralogy, geochemistry and diagenesis of clinoptilolite tuffs (Miocene) in the central Simav graben, Western Turkey. *Clays and Clay Minerals*, **56**, 622–632.

Tschernich, R.W. (1992) *Zeolites of the World*. Geoscience Press, Phoenix, Arizona, USA.

Weisenberger, T. and Spürgın, S. (2009) Zeolites in alkaline rocks of the Kaiserstuhl volcanic complex, SW Germany, new microprobe investigation and the relationship of zeolite mineralogy to the host rock. *Geologica Belgica*, **12**, 75–91.

Winchester, J.A. and Floyd, P.A. (1977) Geochemical magma type discrimination: application to altered and metamorphosed basic igneous rocks. *Earth and Planetary Science Letters*, **28**, 257–272.

(*Received 17 October 2012; revised 12 April 2013; Ms. 719; A.E. S. Kadir*)